ROYAL SOCIETY
OF CHEMISTRY

PAPER

Z-scheme BiVO$_4$/Ag/Ag$_2$S composites with enhanced photocatalytic efficiency under visible light†

Yi Liu, [ID] *[abd] Jiajia Chen,[c] Jinfeng Zhang,[abd] Zhongliang Tang,[a] Haibin Li[a] and Jian Yuan[a]

The Z-scheme BiVO$_4$/Ag/Ag$_2$S photocatalyst was fabricated *via* a two-step route. The as-prepared samples were characterized by XRD, FE-SEM, HRTEM, XPS and UV-vis diffuse reflectance spectroscopy. The results of PL and photocurrent response tests demonstrate that the ternary BiVO$_4$/Ag/Ag$_2$S composites had a high separation and migration efficiency of photoexcited carriers. As a result, the ternary photocatalyst exhibits enhanced photocatalytic activity for decomposing Rhodamine B (RhB) under LED light (420 nm) irradiation. The results of trapping experiments demonstrate both h$^+$ and $^\cdot$OH play crucial roles in decomposing RhB molecules. Additionally, the energy band structures and density of states (DOS) of BiVO$_4$ and Ag$_2$S were investigated *via* the density functional theory (DFT) method. Finally, a Z-scheme electron migration mechanism of BiVO$_4$ → Ag → Ag$_2$S was proposed based on the experimental and calculated results.

1 Introduction

Nowadays, photocatalysis technology is regarded as one of the best ways to alleviate energy and environmental issues. TiO$_2$ is a widely known photocatalyst for water splitting and decomposing organic pollutants. However, TiO$_2$ is only sensitive to UV radiation due to its large bandgap (3.2 eV). Accordingly, a maximum of 6% of solar energy can be harvested using this material, which limits its practical application.[1] This obvious disadvantage is the main motivation for the search for new and more efficient visible-light-driven photocatalysts.

Among the developed photocatalysts, monoclinic structured BiVO$_4$ has emerged as a potentially suitable visible-light-driven photocatalyst because its exceptional properties, such as narrow bandgap, good photocatalytic activity, and nontoxicity. However, the practical applications of BiVO$_4$ is significantly limited owing to the weak charge-transfer rate and rapid recombination of photoinduced charge carriers.[2,3] It has been reported that constructing semiconductor heterojunction structures could promote the photoexcited charge carrier separation, and hence improve the performance of

photocatalyst. Cao *et al.* prepared Au/BiVO$_4$ nanocomposites with excellent activity for water splitting owing to the improved charge separation and surface plasmon resonance of Au nanoparticles.[4] Regmi *et al.* reported that Ag-modified BiVO$_4$ sample exhibits better photocatalytic activity than BiVO$_4$, which can effectively degrade bisphenol A and deactivate the *Escherichia coli*.[5] Li *et al.* synthesized Ag$_3$PO$_4$/BiVO$_4$ composites with type-II heterojunction, which can effectively degrade methylene blue (MB).[6] Li *et al.* reported that the MoS$_2$/BiVO$_4$ composites also show excellent photoactivity for decoloring MB.[7] Similarly, a number of studies of BiVO$_4$ coupled with metal nanoparticles or other oxides were reported for the purpose of improving photocatalytic activity as well, such as Bi/BiVO$_4$,[8] Pd/BiVO$_4$,[9] CdS/BiVO$_4$,[10] g-C$_3$N$_4$/BiVO$_4$,[11,12] Bi$_2$S$_3$/BiVO$_4$,[13] WO$_3$/BiVO$_4$,[14] Ag$_2$O/BiVO$_4$,[15] Cu$_2$O/BiVO$_4$,[16] and BiVO$_4$/RGO.[17]

Ag$_2$S has aroused much research interest owing to its narrow bandgap, which means that it can utilize more energy from the solar light spectrum. Therefore, Ag$_2$S can act as photocatalyst or suitable sensitizer for photocatalysts under visible light irradiation. For example, Ghafoor *et al.* reported that Ag$_2$S nanoparticles photosensitized TiO$_2$ nanofibers display enhanced simulated solar light driven photocatalytic performance.[18] Kumar *et al.* reported that a p–n heterojunction was fabricated by modifying NaNbO$_3$ nanorods with Ag$_2$S particle, which possesses excellent photoelectrochemical and photocatalytic activity.[19] Jiang *et al.* found that compared with g-C$_3$N$_4$, the Ag$_2$S/g-C$_3$N$_4$ photocatalyst exhibits improved activity for H$_2$-evolution. Interestingly, Ag was formed in the process of H$_2$-production. It was suggested that both Ag and Ag$_2$S played a synergistic role in hydrogen production.[20] Guan *et al.* prepared a p–n junction of Ag$_2$S/BiVO$_4$ with significantly improved

[a]College of Physics and Electronic Information, Huaibei Normal University, Huaibei, Anhui, 235000, P. R. China. E-mail: yiliu@chnu.edu.cn

[b]Key Laboratory of Green and Precise Synthetic Chemistry and Applications, Ministry of Education, Huaibei Normal University, Huaibei, Anhui, 235000, P. R. China

[c]College of Chemistry and Materials Science, Huaibei Normal University, Huaibei, Anhui, 235000, P. R. China

[d]Anhui Province Key Laboratory of Pollutant Sensitive Materials and Environmental Remediation, Huaibei Normal University, Huaibei, Anhui, 235000, P. R. China

† Electronic supplementary information (ESI) available. See DOI: 10.1039/d0ra05712f

photoelectrochemical water splitting ability.[21] Zhao *et al.* reported that Ag$_2$S/BiVO$_4$ junction displays a better photocatalytic efficiency with the aid of plasmon resonance of Ag nanoparticles.[22]

However, it is known that the redox ability of photoexcited electrons and holes on reaction sites deteriorated during the charge transfer process in p–n or type-II heterojunction. As a result, the traditional semiconductor heterojunction could not exhibits both excellent charge-separation efficiency and powerful redox ability simultaneously.[23] To overcome this drawback, the Z-scheme photocatalytic system has been developed. It was believed that the Z-scheme photocatalytic system not only promotes the separation of the photo-induced carriers, but also can optimizes carriers redox ability.[24–26] For example, Tada *et al.* reported a Z-scheme CdS–Au–TiO$_2$ composites with high photocatalytic activity, which exhibit an electron migration of TiO$_2$ → Au → CdS.[27] This unique electron migration is different with previously reported CdS/TiO$_2$,[28] which was attributed to the Au nanoparticles acting as the electron mediator. Yin *et al.* reported that C$_3$N$_4$/Cu$_2$O photocatalyst with a p–n heterojunction can be changed to a Z-scheme system C$_3$N$_4$/Pd/Cu$_2$O by inserting metal Pd into the C$_3$N$_4$/Cu$_2$O interface, which has enhanced photocatalytic activity and stability.[29] The inserted Pd nanocubes in the stack structure and the unique design are the critical roles in the formation of Z-scheme system. Deng *et al.* also synthesized a Z-scheme system BiVO$_4$/Ag/Cu$_2$O by deposing metallic Ag to the p–n heterojunction BiVO$_4$/Cu$_2$O.[30] Lin *et al.* reported that a Z-scheme electron migration was confirmed in Ag$_3$PO$_4$/Ag/Bi$_2$MoO$_6$ composites, which is different with typical Ag$_3$PO$_4$/Bi$_2$MoO$_6$ type-II heterojunction.[31,32] Li *et al.* found that the Ag/Ag$_3$PO$_4$/WO$_3$ nanocomposites show better photocatalytic performance than traditional Ag$_3$PO$_4$/WO$_3$ heterojunction, which can be attributed to the formation of Z-scheme structure.[33] Zhao *et al.* prepared Z-scheme g-C$_3$N$_4$/Au/P25 composites with excellent photoactivity by introducing metal Au to the g-C$_3$N$_4$/P25 heterojunction.[34] Liu *et al.* fabricated Z-scheme Cu$_2$O/Au@CeO$_2$ composites with strong redox ability by embedding Au nanoparticles in the yolk–shell Cu$_2$O@CeO$_2$ structure, which can effectively oxidize amines into imines.[35] Bao *et al.* prepared efficient Z-scheme Cu$_2$O/Cu/g-C$_3$N$_4$ photocatalyst for decomposing phenol *via* reduction route, in which partial metal Cu was preserved as a bridge for the transfer of photoexcited charge.[36] Shen *et al.* reported that when reduced graphene oxide was introduced to a Cu$_2$O/Fe$_2$O$_3$ type-II junction, the electron migration of Fe$_2$O$_3$ → RGO → Cu$_2$O was confirmed in the Z-scheme RGO-Cu$_2$O/Fe$_2$O$_3$ composites.[37] Similarly, some Z-scheme photocatalysts were prepared by introducing Ag or Au to a type-II heterojunction, such as Ag$_2$CO$_3$/Ag/AgBr,[38] g-C$_3$N$_4$/Ag/Ag$_3$VO$_4$[39] and Au/TiO$_2$-gC$_3$N$_4$.[40] Therefore, it was possible that a Z-scheme photocatalytic system could be fabricated by properly adding electron mediator to a p–n or type-II heterojunction.

Herein, the Z-scheme system BiVO$_4$/Ag/Ag$_2$S photocatalyst was prepared *via* two-step route in this work. The photocatalytic activity of the synthesized Z-scheme BiVO$_4$/Ag/Ag$_2$S photocatalyst was investigated in this study. Additionally, the possible mechanism of the improved photocatalytic performance of BiVO$_4$/Ag/Ag$_2$S was discussed.

2 Experimental

2.1 Synthesis of photocatalysts

The BiVO$_4$ sample was obtained *via* a previously reported route.[41] 0.3 g BiVO$_4$ and 0.1 mmol AgNO$_3$ were added into 50 mL of distilled (DI) water and stirred for 3 h. Then, the mixture was added with 5 mL of methanol and irradiated by a UV light (100 W) for 1 h. The resulting powders (BiVO$_4$/Ag composites) were collected by centrifuge and washed with DI water and ethanol, then dried at 70 °C for 8 h. 0.3 g as-synthesized BiVO$_4$/Ag composites was ultrasonically dispersed in 50 mL DI water. Then, AgNO$_3$ was added and stirred for 1 h. Subsequently, 50 mL of Na$_2$S solution was dropped into the mixture and stirred for 8 h under dark condition. Similarly, the obtained product was centrifuged, washed and dried, in which the weight ratio of BiVO$_4$, Ag and Ag$_2$S is 100 : 1 : 1.

2.2 Characterization of the as-prepared samples

X-ray diffraction (XRD) was recorded by X-ray diffractometer (Bruker D8) with Cu Kα radiation. The samples' morphologies were characterized by field emission scanning electron microscopy (JSM 6701F) and high-resolution transmission electron microscopy (HRTEM, FEI Tecnai G2 F20 S-TWIN). X-ray photoelectron spectroscopy (XPS) was collected on ESCALAB 250Xi to identify the chemical compositions and the chemical states of the sample. UV-vis diffuse reflectance spectra (DRS) of the samples were acquired using BaSO$_4$ as a reference material by a PerkinElmer Lambda 950 UV-vis spectrophotometer. Steady-state and time-resolved photoluminescence spectra (PL) were performed on FLS 920 fluorescence spectrometer.

2.3 Photoelectrochemical measurements

The photocurrent responses of as-synthesized photocatalysts were investigated on a Zahner PP211 electrochemical workstation in a three-electrode cell. The FTO coated with photocatalysts served as the working electrode. A Pt wire and an Ag/AgCl (saturated KCl) electrode were applied as counter and reference electrode, respectively. The photocurrent measurements were carried out in 0.1 M Na$_2$SO$_4$ solution. A 30 W LED lamp with lighting wavelength of 420 nm was utilized as the light source. The light spectrum of the LED lamp is presented in Fig. S1.†

2.4 Photocatalytic test

The photocatalytic activity of the samples was evaluated by photo-decomposing RhB. The obtained photocatalysts (50 mg) were dispersed into 50 mL RhB aqueous solution (10 mg L^{-1}) and stirred in a dark condition for 30 min to ensure an adsorption–desorption equilibrium before irradiation. A LED lamp (30 W, 420 nm) was used as the visible light source. During the photodegradation experiment, the suspension was under continuous magnetic stirring. 5 mL of reaction solution was taken at 30 min intervals for analysis. The RhB concentration

was monitored by Lambda 950 spectroscopy at a wavelength of 553 nm.

2.5 Computational details

Energy band structures and DOS of $BiVO_4$ and Ag_2S were investigated by the DFT method, in which plane-wave pseudo-potential with CASTEP code was adopted. The generalized gradient approximation with the Perdew–Burke–Ernzerhof was applied as the exchange and correlation terms. The cutoff energies of 450 eV were used for all calculations. Monkhorst–Pack K-points grids of $5 \times 5 \times 2$ and $6 \times 3 \times 3$ were applied for $BiVO_4$ and Ag_2S, respectively.

3 Results and discussion

Fig. 1 presents the XRD patterns of the as-synthesized $BiVO_4$, Ag_2S, $BiVO_4/Ag$ and $BiVO_4/Ag/Ag_2S$ samples. For the $BiVO_4$ and Ag_2S samples, all the peaks could be assigned to $BiVO_4$ (JCPDS 14-0668) and Ag_2S (JCPDS 14-0072) respectively. The XRD patterns of $BiVO_4$, $BiVO_4/Ag$ and $BiVO_4/Ag/Ag_2S$ samples were similar. No diffraction peaks from Ag are observed in the $BiVO_4/Ag$ sample. Similar phenomenon was observed in the XRD pattern of $BiVO_4/Ag/Ag_2S$ sample and Ag_2S was not detected as well. These results can be ascribed to the high crystallinity of $BiVO_4$ powders and low contents of Ag and Ag_2S. To further verify the existence of Ag and Ag_2S, the as-obtained photo-catalysts were further investigated by SEM, HRTEM and XPS.

Fig. 2 shows the SEM, TEM and HRTEM images of the as-obtained products. As shown in Fig. 2a, plate-like $BiVO_4$ powders were obtained, which have a thickness of *ca.* 350 nm. Furthermore, the particles surface is rather smooth and clean. Fig. 2b shows the SEM image of the $BiVO_4/Ag$ composites. Clearly, Ag nanoparticles with diameter of 50–100 nm are attached on the surface of $BiVO_4$. It was suggested that metal Ag was deposited on the plate-like $BiVO_4$ particles. Fig. 2c and d present the SEM images of $BiVO_4/Ag/Ag_2S$ composites with different magnification. In contrast to Fig. 2b, fine nano-particles with a size of *ca.* 5 nm are observed on the $BiVO_4$

particles, which could be referred as Ag_2S nanoparticles formed on $BiVO_4/Ag$ composites. In addition, the TEM and HRTEM images of the $BiVO_4/Ag/Ag_2S$ composites were recorded to further reveal its composition (Fig. 2e–g). In Fig. 2g, the lattice spacing of 0.24 nm and 0.34 nm are corresponded to the crystal plane of Ag (111) and Ag_2S (110), respectively. This result indicates that some Ag_2S nanoparticles were formed on the Ag particles.

X-ray photoelectron spectroscopy (XPS) provided further evidence as to the existence of Ag and Ag_2S in the ternary $BiVO_4/Ag/Ag_2S$ composites. Ag, S, Bi, V and O elements were detected by the XPS survey spectrum of the ternary composites, as presented in Fig. 3a. From high resolution XPS analysis as depicted in Fig. 3b, two strong peaks at 373.5 and 374.2 eV were observed, which are indexed to Ag $3d_{5/2}$ and Ag $3d_{3/2}$, respectively. These two peaks could be fitted by four bands. Two peaks at 368.5 and 374.5 eV correspond to Ag^0 $3d_{5/2}$ and $3d_{3/2}$ respectively, which demonstrated the presence of metal Ag. Another two peaks at 368.0 and 374.0 eV correspond to Ag^+ $3d_{5/2}$ and $3d_{3/2}$ respectively. Furthermore, the peak located at 160.8 eV can be assigned to S 2p binding energy for Ag_2S (Fig. 3c). It demonstrates that both Ag and Ag_2S were contained in the as-prepared $BiVO_4/Ag/Ag_2S$ sample. The Fig. 3d exhibits two peaks at 159.2 and 164.5 eV, which are ascribed to Bi $4f_{7/2}$ and Bi $4f_{5/2}$ of Bi^{3+} in the $BiVO_4$, respectively. Two peaks at 516.9 and 524.3 eV (Fig. 3e) are attributed to V $2p_{3/2}$ and V $2p_{1/2}$ of V^{5+} in the $BiVO_4$, respectively. In Fig. 3f, the O 1s binding energy was observed at about 529.9 eV. The other O 1s peak can be attributed to –OH group or chemisorbed water molecule on $BiVO_4/Ag/Ag_2S$ composites surface. Basing on the XPS result, the SEM and HRTEM images, it was suggested that the ternary $BiVO_4/Ag/Ag_2S$ photocatalyst was successfully fabricated.

Fig. 4a depicts the optical property of the as-prepared samples. It can be found that all $BiVO_4$ based samples showed a strong absorption band in the 420–530 nm wavelength range, which suggested that they can absorb considerable amounts of visible light in this range. Therefore, the as-prepared $BiVO_4$ based samples could act as visible-light-driven photocatalysts. Additionally, the bandgap of photocatalyst can be calculated by the following equation:[42]

$$(\alpha h\nu)^n = A(h\nu - E_g)$$

where α, h, ν, E_g, and A are the absorption coefficient, Planck's constant, the light frequency, the bandgap, and a constant, respectively. $n = 1/2$ is for an indirect transmission; $n = 2$ is for a direct transmission. By plotting $(\alpha h\nu)^{1/2}$ *vs.* $h\nu$ (Fig. 4b), the bandgaps of the $BiVO_4$, $BiVO_4/Ag$, $BiVO_4/Ag_2S$ and $BiVO_4/Ag/Ag_2S$ photocatalysts are evaluated to be 2.40, 2.36, 2.34 and 2.35 eV, respectively. It suggests that the bandgap width of $BiVO_4$ was slightly decreased by co-depositing Ag and Ag_2S nanoparticles.

Fig. 5a displays the PL spectra of $BiVO_4$, $BiVO_4/Ag$, $BiVO_4/Ag_2S$ and $BiVO_4/Ag/Ag_2S$ samples. It is widely accepted that high PL intensity suggests rapid recombination of excited pairs, and results in poor photocatalytic activity. The PL peak located at about 545 nm was recorded for all samples, which was result
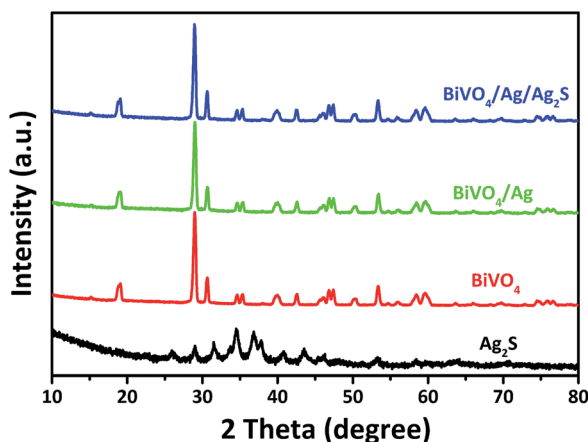

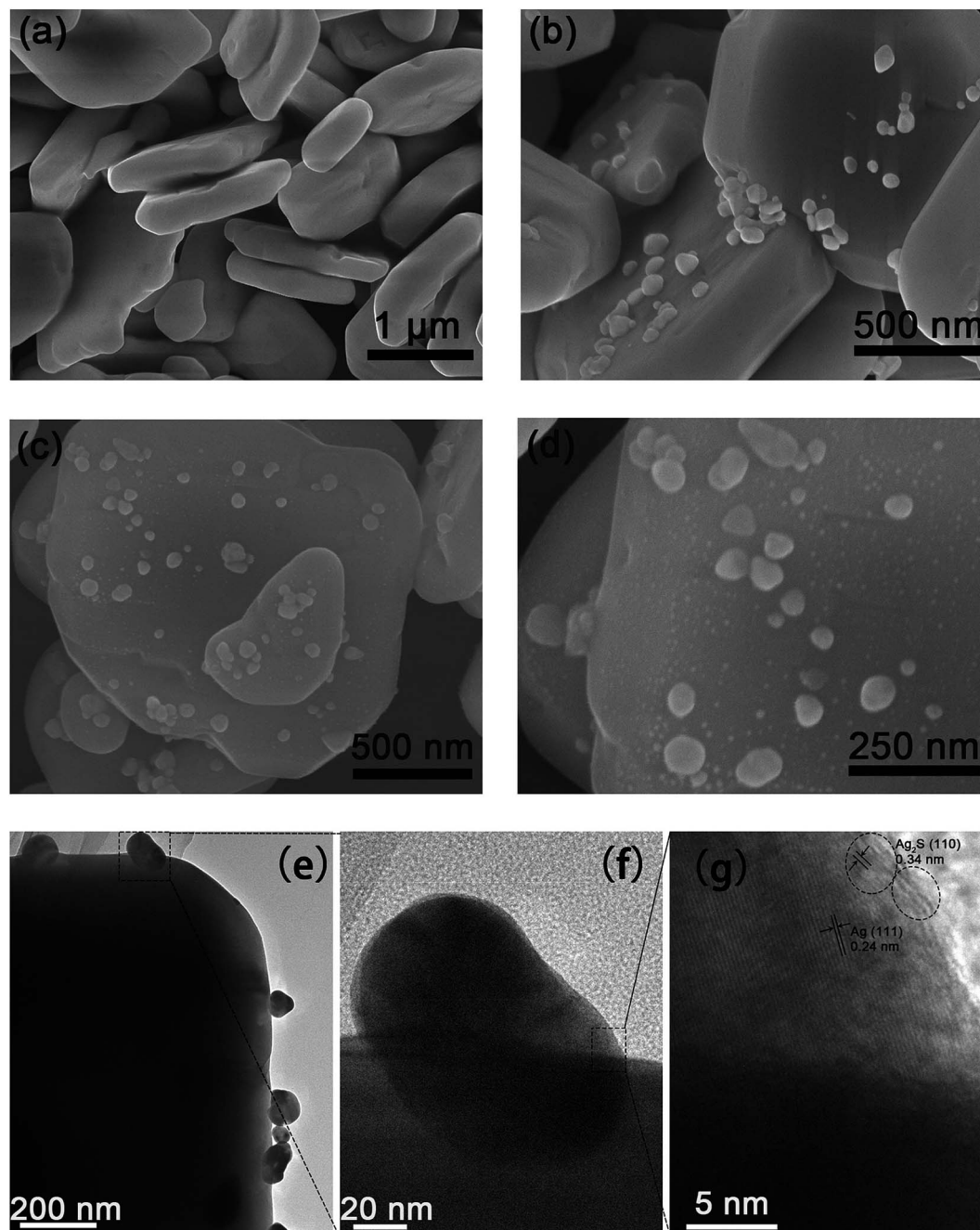**Fig. 1** XRD patterns of the as-obtained Ag_2S, $BiVO_4$, $BiVO_4/Ag$ and $BiVO_4/Ag/Ag_2S$ samples.

Fig. 2 FESEM images of (a) $BiVO_4$, (b) $BiVO_4/Ag$ and (c and d) $BiVO_4/Ag/Ag_2S$, (e and f) TEM and (g) HRTEM images of $BiVO_4/Ag/Ag_2S$ composites.

from the photogenerated carrier recombination in $BiVO_4$ particles. Compared with $BiVO_4$, both the $BiVO_4/Ag$ and $BiVO_4/Ag_2S$ display lower PL intensity, indicating that the recombination of carriers could be suppressed by modifying with Ag or Ag_2S nanoparticles. The ternary $BiVO_4/Ag/Ag_2S$ sample shows the lowest PL intensity, which implying that it has the lowest carrier recombination rate. This is also confirmed by the time-resolved PL spectra (Fig. S2 and Table S1†). It is suggested that the synergistic effect of the Ag and Ag_2S nanoparticles play a key role to promote the separation of photoexcited carriers in the $BiVO_4/Ag/Ag_2S$ composites.

To further understand the separation and migration efficiency of photoinduced electron–hole pairs, the photocurrent responses under dark and LED light irradiation were measured. As shown in Fig. 5b, the photocurrents of the prepared samples were stable and reversible at light-on and light-off. It is well known that larger photocurrent indicated a higher separation efficiency of photoexcited carriers. In comparison with $BiVO_4$, $BiVO_4/Ag$ and $BiVO_4/Ag_2S$, $BiVO_4/Ag/Ag_2S$ composites exhibited the highest photocurrent response density, about 4.5, 2.2 and 1.5 times that of $BiVO_4$, $BiVO_4/Ag$ and $BiVO_4/Ag_2S$, respectively. It indicates that the $BiVO_4/Ag/Ag_2S$ composites exhibit efficient
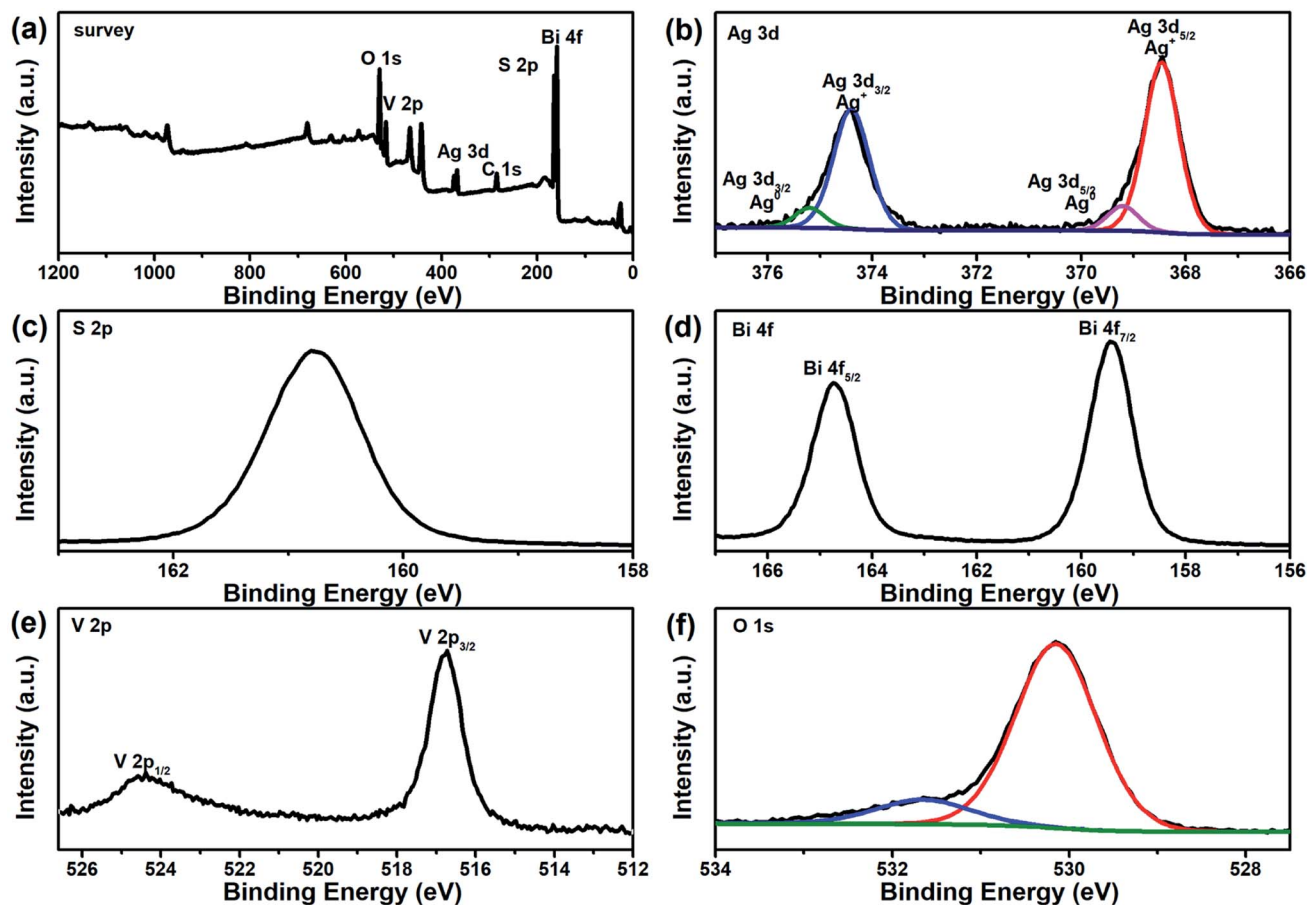
Fig. 3 XPS spectra of BiVO$_4$/Ag/Ag$_2$S composites: (a) survey, (b) Ag 3d, (c) S 2p, (d) Bi 4f, (e) V 2p and (f) O 1s.

charge separation, which is in agreement with the PL spectroscopy results.

Fig. 6a depicts the photoactivity of the as-synthesized catalysts, which was estimated by degrading RhB. When the pure BiVO$_4$ sample was used as photocatalyst, only about 5% of RhB was degraded after 120 min irradiation. For the binary catalysts of BiVO$_4$/Ag and BiVO$_4$/Ag$_2$S, about 39% and 42% of RhB were

degraded, respectively. It indicates that the photocatalytic activity of BiVO$_4$ could be simply enhanced by decorating with Ag or Ag$_2$S nanoparticles. The BiVO$_4$/Ag/Ag$_2$S photocatalyst shows excellent photocatalytic performance compared with other as-prepared samples. About 69% of RhB were degraded by the ternary composites. To directly show the improved photocatalytic activity of BiVO$_4$/Ag/Ag$_2$S sample, the degradation
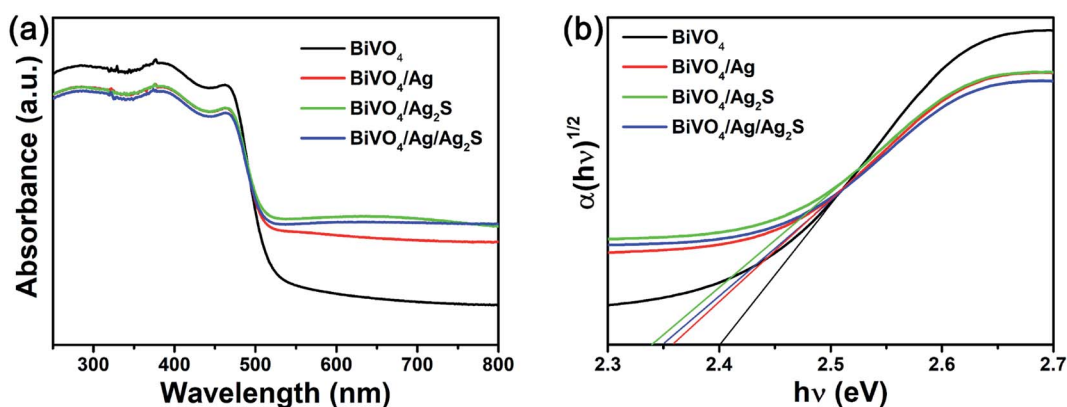

Fig. 4 (a) UV-vis DRS absorption and (b) the plot of $(\alpha h\nu)^{1/2}$ vs. $h\nu$ of the as-obtained BiVO$_4$, BiVO$_4$/Ag, BiVO$_4$/Ag$_2$S and BiVO$_4$/Ag/Ag$_2$S photocatalysts.
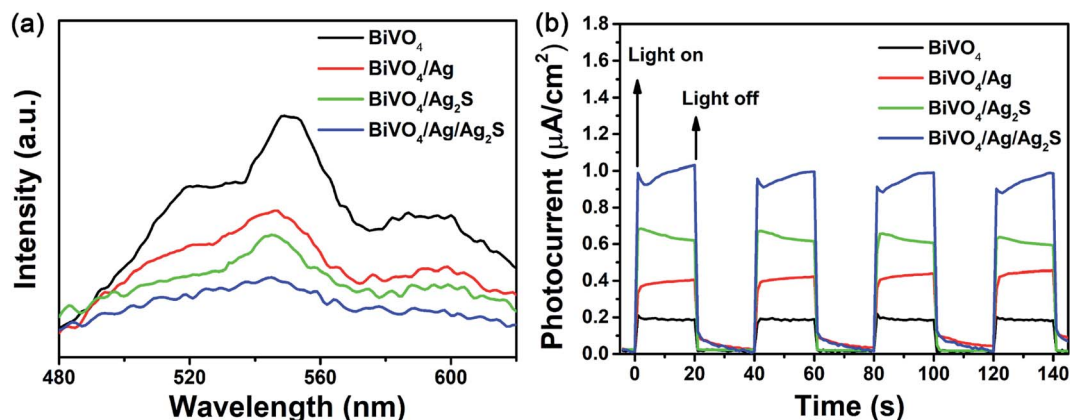
Fig. 5 (a) PL spectrum and (b) photocurrent responses of the as-obtained $BiVO_4$, $BiVO_4/Ag$, $BiVO_4/Ag_2S$ and $BiVO_4/Ag/Ag_2S$ photocatalysts.

kinetics for the removal of RhB were calculated by the pseudo-first-order reaction:

$$\ln C/C_0 = -k \times t$$

where C_0 and C are the concentration of RhB solution after adsorption and at the irradiation time t, respectively, k is the apparent reaction rate constant. As illustrated in Fig. 6b, the rate constants corresponding to $BiVO_4$, $BiVO_4/Ag$, $BiVO_4/Ag_2S$
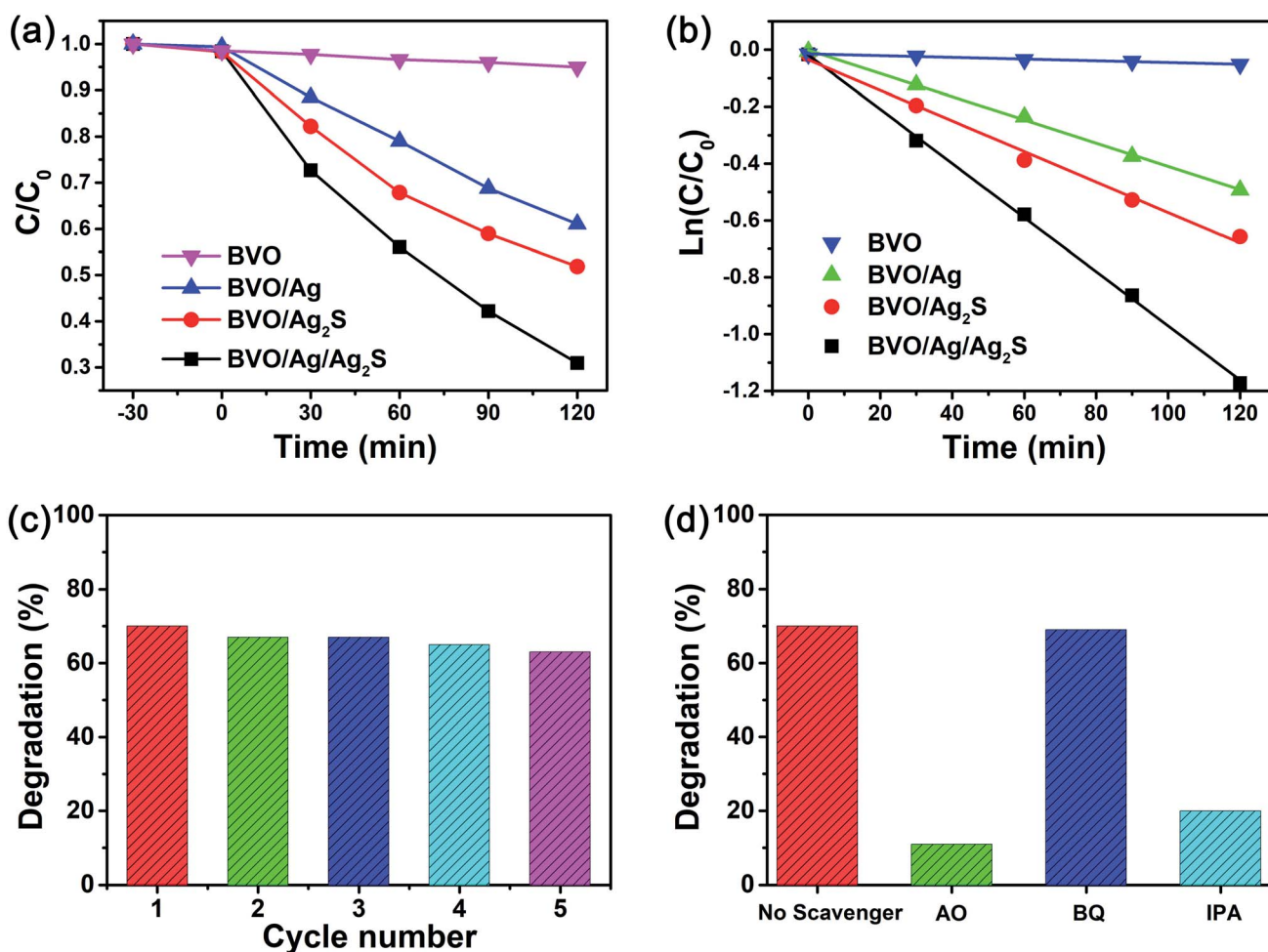

Fig. 6 (a) Photocatalytic activity and (b) kinetic linear simulation curves of the $BiVO_4$, $BiVO_4/Ag$, $BiVO_4/Ag_2S$ and $BiVO_4/Ag/Ag_2S$ samples; (c) the reusability of the $BiVO_4/Ag/Ag_2S$ composites; (d) photodegradation efficiency of RhB over the $BiVO_4/Ag/Ag_2S$ samples by addition of AO, BQ and IPA.

and BiVO$_4$/Ag/Ag$_2$S samples were estimated to be 0.0003, 0.0041, 0.0054 and 0.0095 min^{-1}, respectively. The BiVO$_4$/Ag/Ag$_2$S composites show the highest k value, which is about 1.76, 2.32, 31.7 times higher than that of BiVO$_4$/Ag$_2$S, BiVO$_4$/Ag and BiVO$_4$, respectively. Obviously, the BiVO$_4$/Ag/Ag$_2$S composites shows enhanced photocatalytic efficiency, which can be attributed to the lower electron–hole pair recombination rate and higher photogenerated charge separation efficiency.

The stability of photocatalyst is a crucial issue in its practice application. Fig. 6c shows the recycled experiments of the photodegradation of RhB by using the BiVO$_4$/Ag/Ag$_2$S composites for five cycles (120 min LED light irradiation for each cycle). It can be seen that only slight deterioration of the BiVO$_4$/Ag/Ag$_2$S sample was observed after five cycles, which implies the good recyclability of the prepared photocatalyst.

As is known, the superoxide radical ($^{\cdot}$O^{2-}), holes (h$^+$) and hydroxyl radical ($^{\cdot}$OH) as active species play crucial roles in photocatalytic reaction.[43,44] In order to evaluate the main active species, the trapping experiments were carried out. The reactive species can be removed by adding corresponding scavengers into reaction solutions. The function of different reactive species could be made clear based on the change of photocatalytic performance. In this study, p-benzoquinone (BQ),

ammonium oxalate (AO) and isopropanol (IPA) were added to act as $^{\cdot}$O$_2$$^-$, h$^+$ and $^{\cdot}$OH scavenger, respectively. As presented in Fig. 6d, the ability of the BiVO$_4$/Ag/Ag$_2$S sample to remove RhB was not affected by adding BQ, which suggesting that $^{\cdot}$O$_2$$^-$ radical does not participate in the photocatalytic reaction. However, when BQ and AO were added, the photocatalytic activity of the BiVO$_4$/Ag/Ag$_2$S composites decreased significantly. It demonstrates that h$^+$ and $^{\cdot}$OH play important roles in the photocatalytic process.

To clarify the mechanism of the improved photocatalytic activity of the BiVO$_4$/Ag/Ag$_2$S composites, the band structure of the ternary system was studied. The band edge potentials of valence band (VB) and conduction band (CB) of BiVO$_4$ and Ag$_2$S can be estimated according the following equations:

$$E_{VB} = \chi - E^e + 0.5E_g$$

$$E_{CB} = E_{VB} - E_g$$

where E_{VB} and E_{CB} are the VB and CB edge potential, respectively; χ and E_g are the absolute electronegativity and bandgap energy of the semiconductor, respectively; E^e is fixed at 4.5 V. The E_g of Ag$_2$S is calculated to be 1.46 eV, as shown in Fig. S3,† which is consist with previous report.[45] Thus, the E_{VB} and E_{CB} of
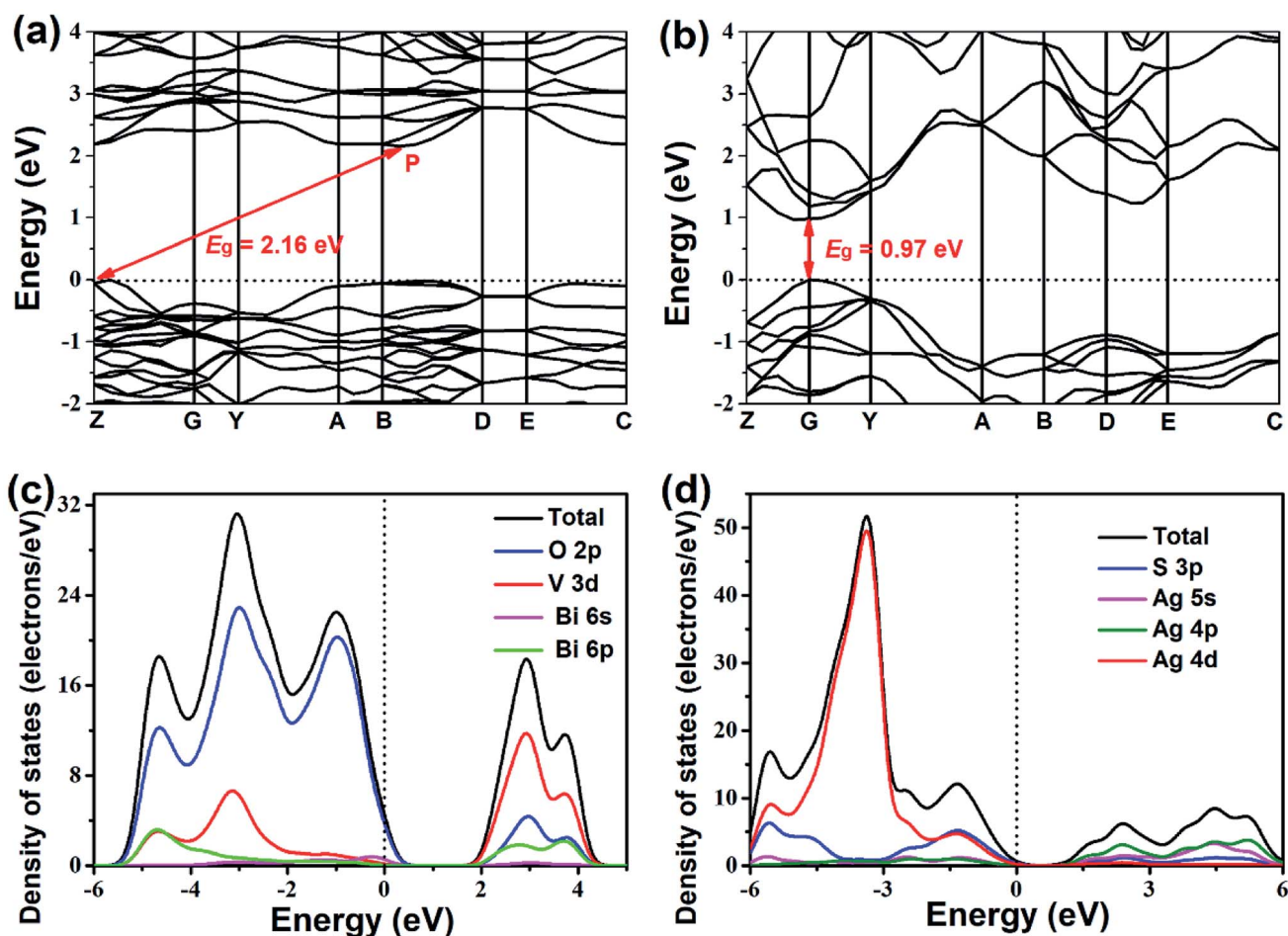

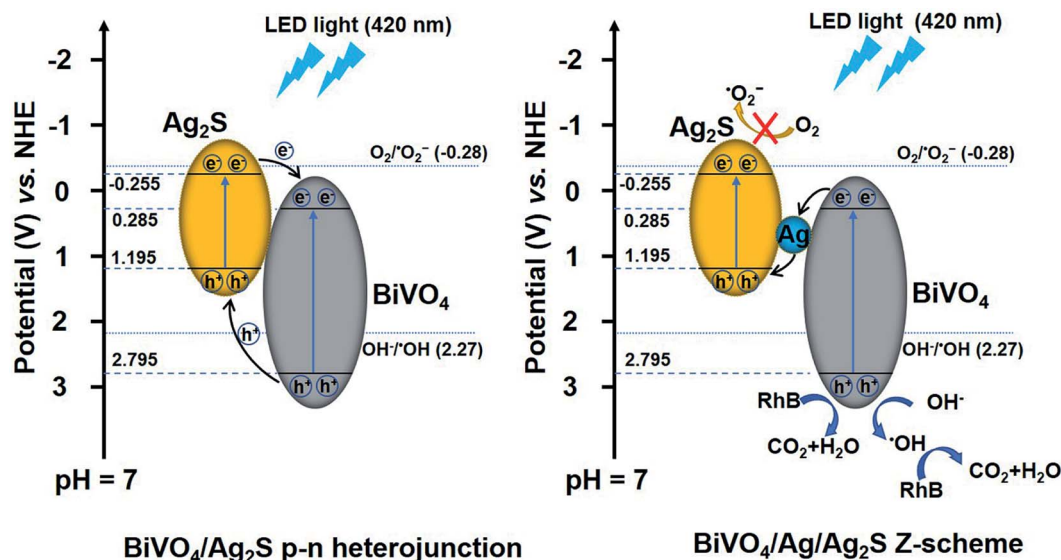Fig. 7 Electronic band structures of (a) BiVO$_4$ and (b) Ag$_2$S and density of states of (c) BiVO$_4$ and (d) Ag$_2$S.

Fig. 8 Schematic illustrating the proposed degradation mechanism of RhB over the ternary $BiVO_4/Ag/Ag_2S$ composites.

Ag_2S are estimated as 1.20 and -0.26 V, *versus* the normal hydrogen electrode (NHE), respectively. Similarly, the E_{VB} and E_{CB} of $BiVO_4$ are 2.795 and 0.285 V, *versus* the NHE, respectively.

Fig. 7 presents the band structures and DOS of $BiVO_4$ and Ag_2S. The valence band maximum (VBM) and conduction band minimum (CBM) are located at Z and P point, respectively (Fig. 7a), which imply that $BiVO_4$ is an indirect bandgap semiconductor. Ag_2S belongs to the direct bandgap semiconductor because the position of VBM is same as that of CBM, as demonstrated in Fig. 7b. The bandgaps of $BiVO_4$ and Ag_2S are calculated to be 2.16 eV and 0.97 eV, respectively. However, these calculated bandgaps are smaller than experimental values (2.40 eV for $BiVO_4$ and 1.46 eV for Ag_2S), which are resulted from the well-known drawback of DFT calculations.[46] As shown in Fig. 7c, the upper VB of $BiVO_4$ consists largely of O 2p, V 3d and a small amount of Bi 6s and Bi 6p states. Meanwhile, the CB of $BiVO_4$ mainly consist of O 2p, V 3d and Bi 6p states. For Ag_2S (Fig. 7d), the upper VB is mainly composed by Ag 4d states and a few of S 3p states, and the CB is mainly occupied by Ag 4p, Ag 5s and S 3p states. It is reasonable that the S 3p states result in the narrow bandgap of Ag_2S.[47]

Based on the above results and discussion, the mechanism of the photodecomposition of RhB with the $BiVO_4/Ag/Ag_2S$ composites is proposed, as shown in Fig. 8. When the ternary $BiVO_4/Ag/Ag_2S$ composites were irradiated by LED light (420 nm), electrons and holes were generated in the CB and VB of $BiVO_4$ and Ag_2S. It is important to notice that the VB potential of Ag_2S (1.195 V *vs.* NHE) is above the ˙OH/OH⁻ potential (2.27 V *vs.* NHE at pH = 7),[48] which demonstrating that the holes photogenerated in the VB of Ag_2S cannot reacted with OH⁻ to produce ˙OH active species. Therefore, it is not supposed that the photoinduced holes transfer from $BiVO_4$ to Ag_2S according to the traditional p–n heterojunction. It is suggested that a Z-scheme electron migration emerges in the ternary photocatalyst. The photoexcited electrons in the CB of $BiVO_4$

transferred to Ag and then recombined with the photoinduced holes in the VB of Ag_2S, which resulting in a better charge separation. The E_{VB} of $BiVO_4$ (3.37 V *vs.* NHE) is below the ˙OH/OH⁻ potential. Hence, the photoexcited holes in the VB of $BiVO_4$ could reacted with OH⁻ to generate ˙OH.[49] Additionally, the holes of $BiVO_4$ can directly oxidized the RhB dye.[8] Consequently, both h⁺ and ˙OH play crucial roles in decomposing RhB molecule, which is consist with the trapping experimental results.

4 Conclusions

The Z-scheme system $BiVO_4/Ag/Ag_2S$ photocatalyst was successfully prepared *via* two-step method. The as-synthesized ternary $BiVO_4/Ag/Ag_2S$ composites exhibit higher separation efficiency and reduction of carrier recombination rate, which result in enhanced photocatalytic efficiency for decomposing RhB under LED light irradiation. The photocatalytic mechanism over the ternary composites was investigated in detail. It is suggested that Z-scheme electron migration of $BiVO_4 \rightarrow Ag \rightarrow Ag_2S$ exists in the ternary system.

Conflicts of interest

There are no conflicts to declare.

Acknowledgements

References

1 H. Xu, S. Ou Yang, L. Q. Liu, P. Reunchan, N. Umezawa and J. H. Ye, *J. Mater. Chem. A*, 2014, **2**, 12642–12661.

2 A. Malathi, J. Madhavan, M. Ashokkumar and P. Arunachalam, *Appl. Catal., A*, 2018, **555**, 47–74.

3 H. L. Tan, R. Amal and Y. H. Ng, *J. Mater. Chem. A*, 2017, **5**, 16498–16521.

4 S. W. Cao, Z. Yin, J. Barber, F. Y. C. Boey, S. C. J. Loo and C. Xue, *ACS Appl. Mater. Interfaces*, 2012, **4**, 418–423.

5 R. Chhabilal, D. Dipesh and L. Soo Wohn, *Nanotechnology*, 2018, **29**, 064001.

6 C. J. Li, P. Zhang, R. Lv, J. W. Lu, T. Wang, S. P. Wang, H. F. Wang and J. L. Gong, *Small*, 2013, **9**, 3951–3956.

7 H. L. Li, K. Yu, X. Lei, B. J. Guo, H. Fu and Z. Q. Zhu, *J. Phys. Chem. C*, 2015, **119**, 22681–22689.

8 Q. F. Jing, X. Y. Feng, J. L. Pan, L. M. Chen and Y. N. Liu, *Dalton Trans.*, 2018, **47**, 2602–2609.

9 L. Y. Wang and Z. Y. Bian, *Chemosphere*, 2020, **239**, 124815.

10 R. Guo, A. G. Yan, J. J. Xu, B. T. Xu, T. T. Li, X. W. Liu, T. F. Yi and S. H. Luo, *J. Alloys Compd.*, 2020, **817**, 153246.

11 J. Safaei, H. Ullah, N. A. Mohamed, M. F. Mohamad Noh, M. F. Soh, A. A. Tahir, N. Ahmad Ludin, M. A. Ibrahim, W. N. R. Wan Isahak and M. A. Mat Teridi, *Appl. Catal., B*, 2018, **234**, 296–310.

12 Z. S. Zhang, M. Wang, W. Q. Cui and H. Sui, *RSC Adv.*, 2017, **7**, 8167–8177.

13 W. Wang, X. W. Wang, C. X. Zhou, B. Du, J. X. Cai, G. Feng and R. B. Zhang, *J. Phys. Chem. C*, 2017, **121**, 19104–19111.

14 C. Yin, S. M. Zhu and D. Zhang, *RSC Adv.*, 2017, **7**, 27354–27360.

15 J. P. Ren and Y. Y. Zhu, *RSC Adv.*, 2020, **10**, 6114–6120.

16 W. Wang, X. Huang, S. Wu, Y. Zhou, L. Wang, H. Shi, Y. Liang and B. Zou, *Appl. Catal., B*, 2013, **134**, 293–301.

17 Y. Wang, W. Wang, H. Mao, Y. Lu, J. Lu, J. Huang, Z. Ye and B. Lu, *ACS Appl. Mater. Interfaces*, 2014, **6**, 12698–12706.

18 S. Ghafoor, S. Ata, N. Mahmood and S. N. Arshad, *Sci. Rep.*, 2017, **7**, 255.

19 S. Kumar, A. P. Singh, C. Bera, M. Thirumal, B. R. Mehta and A. K. Ganguli, *ChemSusChem*, 2016, **9**, 1850–1858.

20 D. L. Jiang, L. L. Chen, J. M. Xie and M. Chen, *Dalton Trans.*, 2014, **43**, 4878–4885.

21 P. Guan, H. Y. Bai, F. G. Wang, H. Yu, D. B. Xu, B. Y. Chen, T. Xia, W. Q. Fan and W. D. Shi, *ChemCatChem*, 2018, **10**, 4941–4947.

22 Z. Wei, D. Ben Lin, Z. Feng Xia, T. Xin Yue, X. Ji Ming, Z. Li Li, L. Shi Yin, D. Y. C. Leung and C. Sun, *Appl. Catal., B*, 2018, **229**, 171–180.

23 P. Zhou, J. G. Yu and M. Jaroniec, *Adv. Mater.*, 2014, **26**, 4920–4935.

24 H. Li, W. G. Tu, Y. Zhou and Z. G. Zou, *Adv. Sci.*, 2016, **3**, 1500389.

25 M. Liu, L. Z. Qiao, B. B. Dong, S. Guo, S. Yao, C. Li, Z. M. Zhang and T. B. Lu, *Appl. Catal., B*, 2020, **273**, 119066.

26 L. X. Zhong, B. D. Mao, M. Liu, M. Y. Liu, Y. Q. Sun, Y. T. Song, Z. M. Zhang and T. B. Lu, *J. Energy Chem.*, 2021, **54**, 386–394.

27 H. Tada, T. Mitsui, T. Kiyonaga, T. Akita and K. Tanaka, *Nat. Mater.*, 2006, **5**, 782–786.

28 N. Qin, Y. H. Liu, W. M. Wu, L. J. Shen, X. Chen, Z. H. Li and L. Wu, *Langmuir*, 2015, **31**, 1203–1209.

29 W. J. Yin, L. J. Bai, Y. Z. Zhu, S. X. Zhong, L. H. Zhao, Z. Q. Li and S. Bai, *ACS Appl. Mater. Interfaces*, 2016, **8**, 23133–23142.

30 Y. C. Deng, L. Tang, G. M. Zeng, C. Y. Feng, H. R. Dong, J. J. Wang, H. P. Feng, Y. Liu, Y. Y. Zhou and Y. Pang, *Environ. Sci.: Nano*, 2017, **4**, 1494–1511.

31 X. Lin, J. Hou, S. S. Jiang, Z. Lin, M. Wang and G. B. Che, *RSC Adv.*, 2015, **5**, 104815–104821.

32 Y. S. Xu and W. D. Zhang, *Dalton Trans.*, 2013, **42**, 1094–1101.

33 Q. Y. Li, F. L. Wang, Y. X. Hua, Y. T. Luo, X. H. Liu, G. R. Duan and X. J. Yang, *J. Colloid Interface Sci.*, 2017, **506**, 207–216.

34 W. R. Zhao, L. H. Xie, M. Zhang, Z. Y. Ai, H. P. Xi, Y. J. Li, Q. M. Shi and J. S. Chen, *Int. J. Hydrogen Energy*, 2016, **41**, 6277–6287.

35 Y. Y. Liu, Y. J. Chen, W. Zhou, B. J. Jiang, X. Zhang and G. H. Tian, *Catal. Sci. Technol.*, 2018, **8**, 5535–5543.

36 Y. C. Bao and K. Z. Chen, *Mol. Catal.*, 2017, **432**, 187–195.

37 H. Q. Shen, G. W. Liu, X. Yan, J. H. Jiang, Y. Z. Hong, M. Yan, B. D. Mao, D. Li, W. Q. Fan and W. D. Shi, *Mater. Today Energy*, 2017, **5**, 312–319.

38 J. J. Li, Y. L. Xie, Y. J. Zhong and Y. Hu, *J. Mater. Chem. A*, 2015, **3**, 5474–5481.

39 J. J. Wu, X. P. Shen, X. L. Miao, Z. Y. Ji, J. H. Wang, T. Wang and M. M. Liu, *Eur. J. Inorg. Chem.*, 2017, **2017**, 2845–2853.

40 C. Marchal, T. Cottineau, M. G. Méndez-Medrano, C. Colbeau-Justin, V. Caps and V. Keller, *Adv. Energy Mater.*, 2018, **8**, 1702142.

41 W. Z. Wang, X. W. Huang, S. Wu, Y. X. Zhou, L. J. Wang, H. L. Shi, Y. J. Liang and B. Zou, *Appl. Catal., B*, 2013, **134**, 293–301.

42 M. A. Butler, *J. Appl. Phys.*, 1977, **48**, 1914–1920.

43 H. B. Fu, C. S. Pan, W. Q. Yao and Y. F. Zhu, *J. Phys. Chem. B*, 2005, **109**, 22432–22439.

44 G. Sivalingam, K. Nagaveni, M. S. Hegde and G. Madras, *Appl. Catal., B*, 2003, **45**, 23–38.

45 S. I. Sadovnikov, Y. V. Kuznetsova and A. A. Rempel, *Nano-Struct. Nano-Objects*, 2016, **7**, 81–91.

46 J. P. Perdew and M. Levy, *Phys. Rev. Lett.*, 1983, **51**, 1884–1887.

47 K. Zhang and L. j. Guo, *Catal. Sci. Technol.*, 2013, **3**, 1672–1690.

48 M. Kaneko and I. Okura, *Photocatalysis: science and technology*, Springer, 2002.

49 C. S. Turchi and D. F. Ollis, *J. Catal.*, 1990, **122**, 178–192.